First-principles calculation of capacitance including interfacial effects

Bora Lee,[1] Choong-Ki Lee,[1] Seungwu Han,[1,a)] Jaichan Lee,[2] and Cheol Seong Hwang[3]
[1]*Department of Physics, Ewha Womans University, Seoul 120-750, Republic of Korea*
[2]*School of Materials Science & Engineering, SungKyunKwan University, Suwon 440-746, Republic of Korea*
[3]*School of Materials Science and Engineering, and Inter-University Semiconductor Research Center, Seoul National University, Seoul 151-742, Republic of Korea*

(Received 6 September 2007; accepted 14 November 2007; published online 31 January 2008)

An efficient computational method is proposed within a first-principles framework to calculate capacitances of metal-insulator-metal structures including interfacial effects. In this approach, we employ metal-insulator models under external electric fields to calculate dielectric responses near the interface region. Macroscopically averaged potentials allow for evaluating the capacitance and local dielectric constants of the corresponding metal-insulator-metal capacitor. We apply this method to calculate the capacitance of Au/MgO(100)/Au and $Ni/ZrO_2(110)/Ni$ with dielectric thicknesses of nanometers. While the Au/MgO interface is relatively free of interfacial effects, the computational results for Ni/ZrO_2 indicate the presence of interfacial regions with dielectric constants noticeably lower than that of the bulk. Microscopic origins are discussed. © *2008 American Institute of Physics*. [DOI: 10.1063/1.2832413]

I. INTRODUCTION

The dielectric constant is a fundamental quantity that characterizes electrical and optical responses of insulators. Experimentally, it can be measured with a high precision when materials are in bulk phases. However, for microelectronic devices or thin-film structures, where insulators are vastly employed, dielectric constants are often scattered depending on growth conditions and measurement techniques. Furthermore, it is observed that dielectric constants in metal-insulator-metal (MIM) capacitors are affected by the dielectric thickness[1] or the species of electrodes.[2] This implies that the interface between insulators and metals substantially modify overall dielectric behaviors, which can be understood by high ratios of interface to volume for thin films. However, the understanding of the interfacial effects on dielectric constants is often hampered by difficulties in characterizing interfacial structures, and it is ambiguous whether the variations in dielectric constants are intrinsic or, for instance, due to the existence of a secondary phase near the interface. As individual components are aggressively scaled down for advanced electronic devices, understanding of the interface property is not only a fundamentally intriguing issue but also crucial for the development of reliable electronic devices.

On the theoretical side, a direct study on dielectric properties of capacitors is complicated by the inherent nonequilibrium condition; the applied bias splits chemical potentials of constituent electrodes. However, this is not compatible with the conventional density functional methods to calculate the ground-state properties since they require a unique Fermi level throughout the whole system.[3] Methods based on the nonequilibrium Green's functions can describe the finite bias, but they are still computationally demanding. Recently, Stengel *et al.* noticed that the localized character of Wannier functions can be used to calculate dielectric constants of MIM structures.[4] By applying this method to the interfaces between $SrTiO_3$ and various electrodes, they were able to reveal the presence of dielectric dead layers intrinsic to the metal-oxide interfaces.[5]

In this article, we propose an alternative computational framework based on the first-principles method to calculate dielectric properties or capacitances in consideration of the metal-insulator interface. The simulation of the nonequilibrium condition is enabled by adopting a metal-insulator (MI) slab with both ends exposed to the vacuum, rather than periodically repeated MIM structures. The external bias or potential differences between electrodes are emulated by the application of an electric field. Our method exploits features that are already implemented in widely used first-principles codes such as the VIENNA *AB INITIO* SIMULATION PACKAGE (VASP),[6] or QUANTUM-ESPRESSO[7] and therefore could be employed easily. This paper is organized as follows. In Sec. II, we will outline basic ideas of our theoretical approaches, followed by a detailed computational setup. Exemplary applications to model interfaces of Au/MgO and Ni/ZrO_2 are presented in Sec. III with related discussions. Section IV summarizes the main achievements.

II. COMPUTATIONAL METHODS

A. Basic models

Our method is based on the similarities between a MIM capacitor and its derived metal-insulator (MI) slab, as illustrated in Fig. 1. The starting model in Fig. 1(a) schematically represents a typical capacitor connected to an external voltage source. The interfacial regions with an electrical polarizability distinct from the bulk are explicitly described. The applied bias builds up free charges at the metal-insulator interface, which in turn induces dielectric polarizations inside the insulator. Discontinuities in the polarization also result in

a)Author to whom correspondence should be addressed. Electronic mail: hansw@ewha.ac.kr.

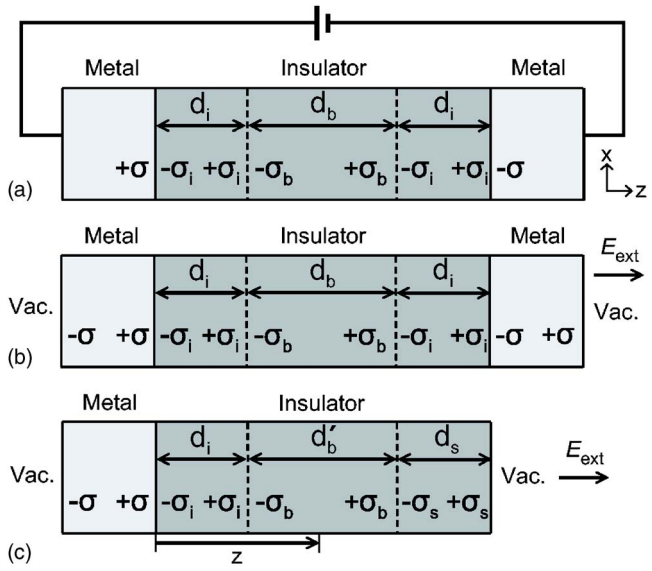

FIG. 1. (Color online) Schematic pictures explaining the computational framework. (a) A conventional MIM capacitor connected to an external voltage source. (b) The electric bias is replaced by an external field which produces the same surface charge density σ as in (a). (c) The metallic electrode on the right-hand side is removed from the MIM model in (b). All constituent materials and interface types are assumed to be identical among model systems.

effective surface charges at various interfaces present in the model system. The capacitance of this model is then calculated in SI units as follows:

$$C_{\mathrm{MIM}} = \frac{\varepsilon_0 \sigma A}{2(\sigma - \sigma_i)d_i + (\sigma - \sigma_b)d_b}, \tag{1}$$

where ε_0 is the vacuum permittivity, σ and d are the surface charge density and thickness of each region, respectively, and A is the cross-sectional area of the electrode. The subscripts i and b in Eq. (1) indicate the interfacial and bulk regions.

The role of the external power source in Fig. 1(a) can be replaced by the external field (E_{ext}) applied on the MIM slab model with both ends exposed to the vacuum [see Fig. 1(b)]. The nonequilibrium condition is maintained as long as the charge transfer between metal electrodes is forbidden.[3] However, as mentioned in the Introduction, this is difficult to achieve within the conventional first-principles calculations. E_{ext} is chosen such that the surface charge density (σ) induced on the metal surface is identical to that in Fig. 1(a). Then, the other parameters (σ_i, σ_b, d_i, and d_b) would not change either. If repeated along the surface normal without the vacuum space, the resulting periodic MIM structure is similar to that used in Refs. 4 and 5.

By removing the right electrode in the isolated MIM model, one arrives at a MI slab model shown in Fig. 1(c), which constitutes the base model used in this work. With the same choice of materials and interface types as in the original MIM capacitor model, the interface properties represented by σ_i and d_i are equal to those in Fig. 1(a). We then define a virtual capacitance $\tilde{C}_{\mathrm{MI}}$ of the MI model as follows:

$$\tilde{C}_{\mathrm{MI}}(z) = \frac{\sigma A}{2V(z)} = \frac{\varepsilon_0 \sigma A}{2(\sigma - \sigma_i)d_i + 2(\sigma - \sigma_b)(z - d_i)}, \tag{2}$$

where $V(z)$ is the potential at z from the interface [see Fig. 1(c)] and evaluated with respect to the potential value inside the metal electrodes. We note that the surface region in Fig. 1(c) (represented by the index s) does not contribute to $\tilde{C}_{\mathrm{MI}}$ as far as surface effects are negligible at z. By equating Eq. (2) with Eq. (1), a condition, $2z = 2d_i + d_b = d$, is obtained where d is the total thickness of the insulator in the MIM model. That is to say, by evaluating $V(z)$ and σ, one can calculate the capacitance of the corresponding MIM structure with an insulator thickness of $2z$. Furthermore, σ is readily obtained from the condition that the electric field vanishes inside the electrodes, which gives $\sigma = \varepsilon_0 E_{\mathrm{ext}}$. Although the model systems in Fig. 1 assume discrete interfacial regions, it is straightforward to extend the above formulation to the case of continuously varying polarizations.

B. First-principles implementations

The schematic framework in the previous section can be implemented within the density functional methods. An atomistic model is first built up representing the metal-insulator interface with both ends exposed to the vacuum, and a constant electric field is applied. To be consistent with the MI model in Fig. 1(c), it should be confirmed that three kinds of electron transfers do not occur under external fields: (i) The electron transfer from the metal to conduction bands of the insulator (Schottky emission). (ii) The transition from valence bands to conduction bands of insulators (Zener breakdown). (iii) The emission of electrons from the metal or insulator to the vacuum (field emission). These conditions can be verified directly by inspecting the distribution of charge densities and partial density of states.

To obtain $V(z)$ in Eq. (2) from first-principles results, it is required to make the atomically varying potentials smooth. The local potential is first averaged over the plane perpendicular to the surface normal. To extract information relevant to dielectric responses, we calculate the change in electrostatic potentials upon the application of electric fields,

$$\Delta V(z) = \frac{1}{L_x L_y} \int_0^{L_x} dx \int_0^{L_y} dy [V_{\mathrm{loc}}(x,y,z;E_{\mathrm{ext}}) - V_{\mathrm{loc}}(x,y,z;0)], \tag{3}$$

where L_x and L_y are the unit cell lengths along the x and y directions, and $V_{\mathrm{loc}}(x,y,z;E)$ is the sum of ionic and Hartree potentials under an external field of E. The ions could be fixed to their equilibrium positions at zero bias or relaxed in response to the finite electric fields. Each corresponds to the dielectric response at optical frequencies (ε^{∞}) or for static fields (ε^{0}), respectively. When ionic relaxations are considered to calculate ε^0, $\Delta V(z)$ is oscillatory due to small displacements of ions. This can be smoothened through a macroscopic average[8] along the z-direction,

$$\langle \Delta V(z) \rangle = \frac{1}{l_1 l_2} \int_{z-(l_1/2)}^{z+(l_1/2)} dz' \int_{z'-(l_2/2)}^{z'+(l_2/2)} dz'' \Delta V(z''), \tag{4}$$

where l_1 and l_2 are the periodicity lengths along the z-direction for the metal and insulator in bulk phases, respectively. As will be shown below, $\langle \Delta V(z) \rangle$ changes smoothly inside the electrodes and insulators, thereby allowing for assigning potential values $[V(z)]$ inside the insulator to be used in Eq. (2). In addition, one can define local dielectric constants as follows:

$$\langle \varepsilon(z) \rangle = E_{\text{ext}} / \frac{d}{dz} \langle -\Delta V(z) \rangle. \tag{5}$$

The concept of local dielectric constants was first introduced for periodic insulating systems in Refs. 9 and 10. In those works, the permittivity profiles were evaluated from local polarizations which were in turn obtained by induced charge densities. In the present formulation, the differential electrostatic potential in Eq. (3) is contributed by the same induced charges. Therefore, the local dielectric constant defined in Eq. (5) is equivalent to that formulated in Ref. 9. The only difference that can be expected is from technical details such as how the potentials or charge densities are averaged. In passing, we add that the above computational approach can be used to evaluate dielectric constants of bulk insulators as long as the slab is thick enough.

One of the advantages in our method is that it can be easily adopted using conventional codes without any major modification. However, some technical considerations are required for free surfaces of insulators present in the model system. (This was also noted in Ref. 4.) If the bulk-terminated surface of the insulator is polar, a surface passivation is required to satisfy electron counting rules and make the surface insulating. This can be achieved in various ways. As an example, attaching hydrogen atoms makes MgO(111) surface insulating.[11] Alternatively, one can control the stoichiometry to neutralize the surface. For instance, the cubic-ZrO_2(100) surface becomes insulating if one oxygen atom is removed from the O-terminated surface unit cell. As another example, the AlO_2 face of the $LaAlO_3$(100) surface can be neutralized by removing one oxygen atom from the (2×2) surface unit cell. For ferroelectric materials, however, the bulk property may not be recovered inside the slab.[12] Therefore, extra caution is demanded when calculating on ferroelectric-metal interfaces.

C. Model systems

For specific models to apply our methods, we choose Au/MgO(100) and Ni/cubic-ZrO_2(110) interfaces (see Fig. 2). The numbers of atoms within the unit supercell are 34 and 65 for Au/MgO and Ni/ZrO_2, respectively. The lattice mismatch between the metal and oxide is within 1% and the in-plane lattice parameters are set to those of oxides. For density functional calculations, we employ VASP throughout this work. The ionic potentials are described by the projector-augmented-wave method,[13] and the exchange-correlation energies of electrons are described within the local density approximation.[14] The energy cutoff of 400 eV is used to generate a plane-wave basis set to expand the wave functions. For the k-point integration, $6\times6\times1$ and $4\times6\times1$ regular meshes are used for Au/MgO and Ni/ZrO_2, respectively. The density of states is broadened by the Gaussian function with a width of 0.05 eV. The vacuum lengths between neighboring supercells are longer than 14 Å to avoid the wave function overlap. The external bias is simulated with a sawtooth potential to be compatible with periodic boundary conditions. The external field induces dipole moments within the model slab, giving rise to spurious long-range dipole-dipole interactions between model slabs. In order to prevent the cross talk between supercells, artificial dipoles are introduced in the middle of the vacuum region to cancel out dipole fields from other slabs.[15] The atomic coordinates are relaxed until the Hellmann-Feynman forces for each atom are reduced to within 0.02 eV/Å.

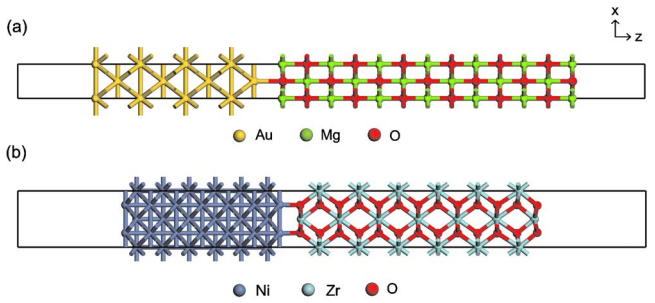

FIG. 2. (Color online) The model interfaces calculated in this work. (a) Au/MgO(100); (b) Ni/ZrO_2(110).

III. RESULTS AND DISCUSSIONS

A. Au/MgO(100) interface

We first discuss on computational results for the Au/MgO(100) interface. The equilibrium geometry indicates that the distance between the outermost metal layer and the Mg(O) atom in the adjacent layer is 2.46 (2.51) Å. Figure 3(a) shows $\langle \Delta V(z) \rangle$ when an external field of 0.1 V/Å is applied along the normal direction of the interface (z-direction). The solid line indicates results obtained with fixed ionic positions while the dashed line is calculated with all atoms fully relaxed. The smooth change of $\langle \Delta V(z) \rangle$ throughout the model system permits an unambiguous determination of capacitances following the formulation given in the previous section. The almost flat potential in the metallic region is indicative of the perfect metallic screening. Inside the insulator, on the other hand, the external field is screened by induced dipole moments, and the internal fields are about 0.03 and 0.01 V/Å for fixed and relaxed results. In Fig. 3(b), field-induced redistributions of charge densities are displayed. The accumulation of electronic charges at the surface of the metal electrode is calculated to be 4.71×10^{-3} $e/\text{Å}^2$ in comparison with 4.83×10^{-3} $e/\text{Å}^2$ estimated directly from the external electric field (see above).

In Fig. 4(a), the inverse of local dielectric constants ($\langle \varepsilon(z) \rangle^{-1}$) is shown. On the metallic side, $\langle \varepsilon(z) \rangle^{-1}$ is close to zero, consistent with the perfect metallic screening. Inside the dielectric, on the other hand, $\langle \varepsilon(z) \rangle^{-1}$ rapidly converges to a finite value. The optical and static dielectric constants

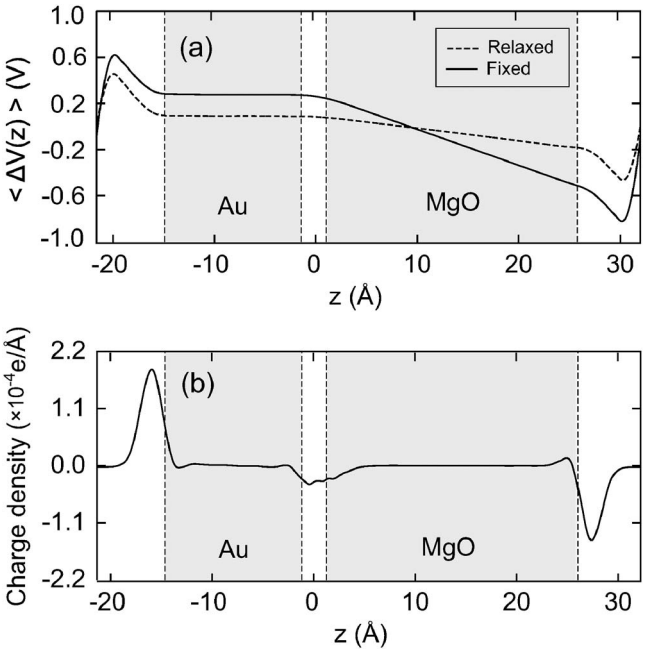

FIG. 3. (a) $\langle \Delta V(z) \rangle$ for the Au/MgO(100) model slab. The external field is 0.1 V/Å. The vertical dashed lines indicate the position of boundary layers of the insulator and the metal. (b) The induced charge density is shown. The ions are fixed to their equilibrium positions.

evaluated in the middle of the MgO slab are 3.36 and 9.65, respectively. These values as well as the profile of $\langle \varepsilon(z) \rangle^{-1}$ in Fig. 3(a) are in good agreement with the results for the corresponding Ag/MgO/Ag capacitor in Ref. 4 calculated with Wannier functions, suggesting that interface properties are well captured in our methods.

The inverse capacitance per unit area and the nominal dielectric constant, which is equal to dC/A, are calculated with respect to the dielectric thickness of the corresponding Au/MgO/Au capacitor. Figure 4(b) shows the results at high frequencies obtained from $\langle \Delta V(z) \rangle$ with fixed ionic positions, while the fully relaxed results are employed to obtain the plots in Fig. 4(c). To define the insulator thickness, the origin corresponding to $z=0$ is set to the middle of the interface layers (see Fig. 3). We recall that the thickness (d) is equal to $2z$ if $V(z)$ is used in evaluating the capacitance based on Eq. (2).

For the sake of analysis, we schematically represent the capacitance including interface regions as follows:

$$\frac{1}{C} = \frac{1}{C_i} + \frac{1}{C_b} + \frac{1}{C_i} = \frac{1}{A\varepsilon_0}\left[2d_i\left(\frac{1}{\varepsilon_i} - \frac{1}{\varepsilon_b}\right) + \frac{d}{\varepsilon_b}\right], \tag{6}$$

where d_i is the interface thickness, and $\varepsilon_i(\varepsilon_b)$ indicates the dielectric constants for the interfacial (bulk) regions, respectively. Equation (6) means that the A/C-vs-d graph crosses the origin if the interfacial effects are negligible ($d_i=0$ or $\varepsilon_i=\varepsilon_b$). In fact, it can be observed in Figs. 4(b) and 4(c) that the extrapolated inverse capacitances narrowly pass through the origin, indicating that the thickness of the interfacial regions is small for both optical and static frequencies. Consistently, the nominal dielectric constants are almost constant with respect to d, as shown in the same figures. The effective dielectric constants ε_b obtained from linear fits of $(C/A)^{-1}$ vs d are 3.22 and 9.56 for optical and static results, respectively, in good agreement with 3.36 and 9.65 obtained directly from $\langle \varepsilon(z) \rangle$.

B. Ni/ZrO_2 interface

For another application, we calculate on Ni/cubic-ZrO_2(110) as shown in Fig. 2(b). ZrO_2 is a candidate replacement oxide to be used in future microelectronic devices.[16] The relaxed structure shows that the Zr and O atoms in the interface layer are at distances of 1.95 and 1.87 Å from the boundary of the electrodes, respectively. The buckling tendency is opposite to that of the Au/MgO interface where the cation is closer to the metal (see above), and this reflects that the surface reactivity is higher for

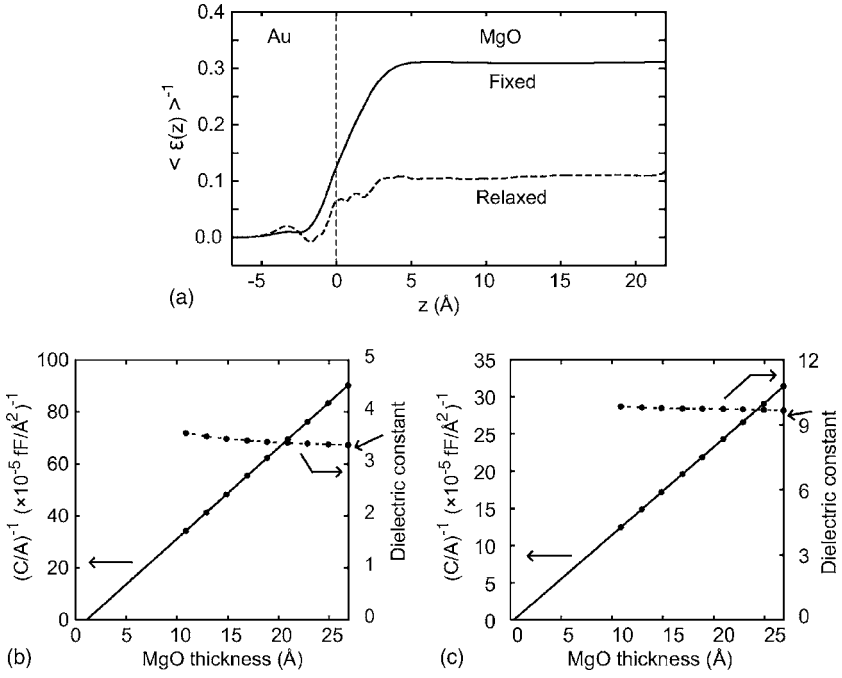

FIG. 4. (a) The inverse of local dielectric constants for the Au/MgO(100) interface with ions fixed (solid line) or relaxed (dashed line). (b) The inverse capacitances and nominal dielectric constants at optical frequencies are shown with respect to the thickness of MgO in the corresponding symmetric Au/MgO/Au capacitor. The bulk dielectric constant is indicated by an arrow on the right axis. (c) Similar graphs at the static frequency.

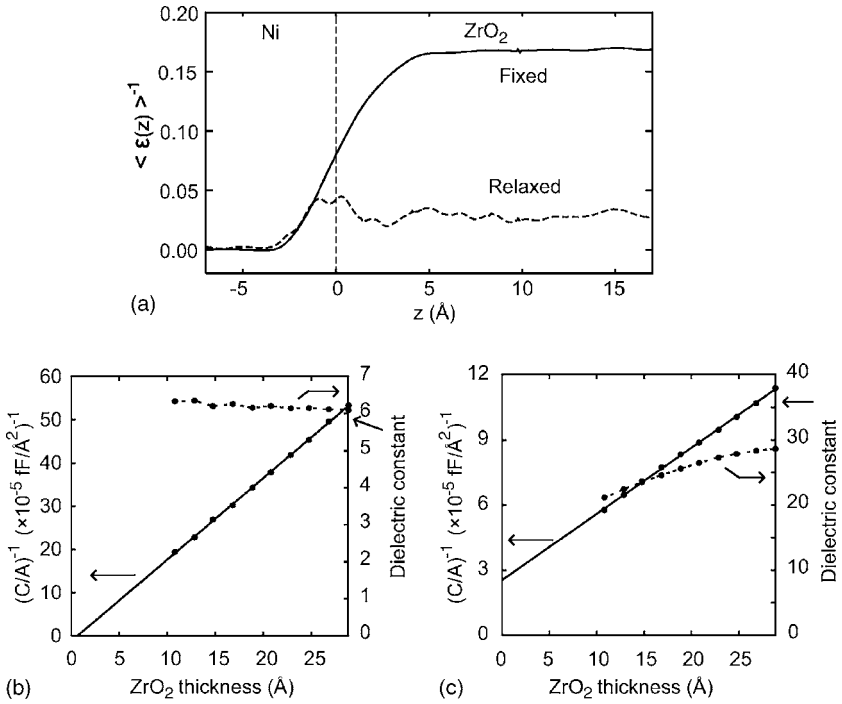

FIG. 5. (a) The inverse of the local dielectric constant for $Ni/ZrO_2(110)$ interface. (b) The inverse capacitances and nominal dielectric constants at optical frequencies are shown with respect to the thickness of ZrO_2 in the corresponding symmetric $Ni/ZrO_2/Ni$ capacitor. The bulk dielectric constant is indicated by an arrow on the right axis. (c) Similar graphs at the static frequency.

$ZrO_2(110)$ than MgO(100). In addition, it is found that the local structures are slightly distorted from the cubic phase to the tetragonal phase. This is due to the unstable phonon mode in cubic ZrO_2 triggering a transition into the tetragonal phase. However, the relative oxygen displacement is only 0.0005 in comparison with the theoretical value of 0.04 in the crystalline tetragonal phase.[17] Therefore, material properties are expected to be very close to those of the cubic phase. In Fig. 5(a), we plot the inverse of the computed $\langle\varepsilon(z)\rangle$. The dielectric constants measured in the middle of ZrO_2 are 6.23 and 36.1 for ε^{∞} and ε^{0}, respectively. These values are in good agreement with 5.75 and 35.52 calculated using the Born effective charges and phonon modes at the zone center.[17] On the other hand, it is noticeable that the dielectric constants are substantially reduced near the interface region. This is contrasted to the fixed results, which show a monotonic transition from the metal to dielectric and therefore do not show interfacial effects in the inverse capacitance curve in Fig. 5(b). Due to the presence of the low-permittivity regions at the interface, the dielectric constants in Fig. 5(c) are substantially smaller than the bulk value when ZrO_2 is thinner than 2 nm. Consistently, the inverse capacitance is extrapolated to a finite value at the zero thickness, which suggests the presence of an interfacial layer based on Eq. (6). The dielectric constant calculated from the slope of the inverse capacitance is 37.1, close to the value of 36.1 above. [The slope of the inverse capacitance in Fig. 5(b) results in ε^{∞} of 5.97 in accord with the value of 5.75 above.]

To gain some insight into the origin of the reduced interfacial dielectric constants for Ni/ZrO_2, we carry out a further analysis on the computational results. First, the screening property of electrodes is checked because the incomplete metallic screening can give rise to interfacial capacitances.[18] To this end, we note that the interfacial effects are not significant for the optical dielectric constants [see Fig. 5(b)], although the $\langle\varepsilon(z)\rangle^{-1}$ profile from the interface ($z=0$) into the metal side is very close to that for the static dielectric constants. Therefore, it can be concluded that the reduction of the dielectric constants for Ni/ZrO_2 originates from the material properties of ZrO_2 at the interface region that are at variance with the bulk.

In general, the ionic parts of static dielectric constants are determined by effective charges and frequencies of the phonon modes related to dielectric relaxations. Therefore, any changes in these quantities lead to variations in the dielectric constants. In Ref. 5, for example, it was shown that the hardening of the soft phonon modes in $SrTiO_3$ is the main origin of the intrinsic dead layer pertaining to the metal-$SrTiO_3$ interfaces. The investigation of the local phonon modes at the interface is beyond the scope of the current work. Instead, we examine the spatial variations of effective charges. In Figs. 6(a) and 6(b), the zz components of Callen dynamical charges (Z_I^C) are shown for the atom I in the insulator part.[9,19] In our model systems, Z_I^C is computed by the z-component of the Hellmann-Feynman force divided by the external field. As shown in Figs. 6(a) and 6(b), the Callen charges are significantly smaller at the interface region. However, the Callen charges are affected by local electric fields, and we calculate in Figs. 6(c) and 6(d) another effective charge $\zeta_I=\varepsilon^{\infty}(z_I)Z_I^C$ that is directly related to effective ionic polarizabilites.[9] It is notable that ζ_I is almost constant from the interface to the bulk for both the Au/MgO and Ni/ZrO_2 interfaces. (However, a slight decrease of ζ_I is noted for the O atom at the Au/MgO interface.) This strongly suggests that the reduction of dielectric constants in Ni/ZrO_2 is likely to be caused by hardening of the soft modes in cubic ZrO_2. Further analysis on local phonon modes will be able to verify this.

IV. SUMMARY

To summarize, we have proposed a simple but efficient first-principles approach to calculate dielectric constants in

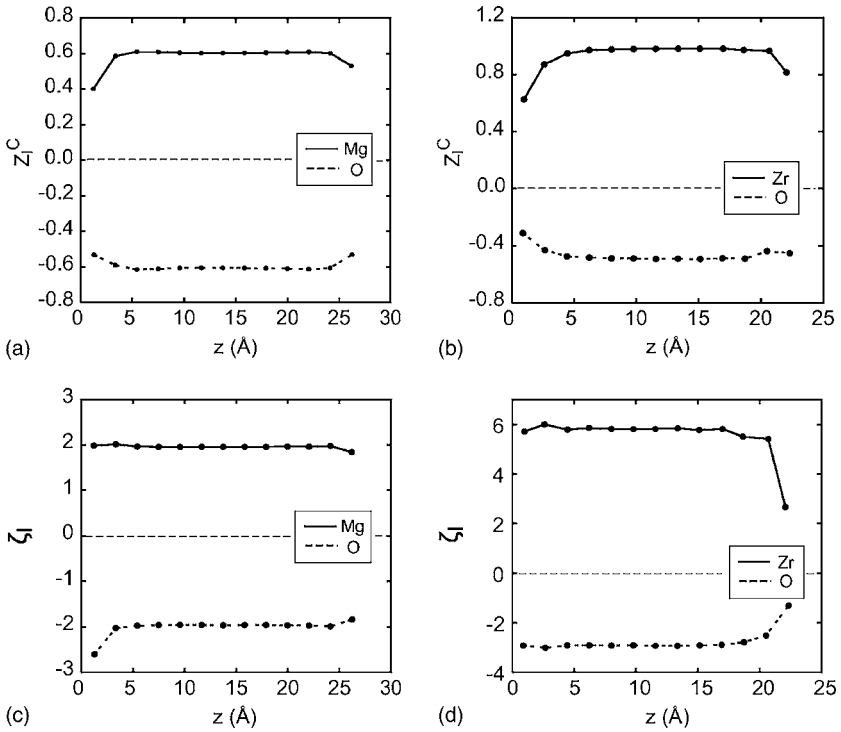

FIG. 6. (a), (b) The *zz* component of Callen charge (Z_I^C) for the atom *I* at a distance *z* from the interface of Au/MgO and Ni/ZrO_2, respectively. (c), (d) Effective charges ζ_I obtained by multiplying Z_I^C with optical dielectric constants at the ionic position for Au/MgO and Ni/ZrO_2, respectively.

consideration of interfacial effects. Our results were in good comparison with the available results obtained by Wannier functions. In the case of a Au/MgO interface, the interfacial effect was negligible, while the local dielectric constant for a Ni/ZrO_2 interface shows a signature of intrinsic dead layers. The effective charges are almost constant throughout the model systems except for the surface region. This implies that the hardening of phonon modes should be the most important origin.

ACKNOWLEDGMENTS

This work was supported by the System IC2010 program of the Korean government and by the KOSEF through National Research Laboratory (NRL) program. The authors would like to acknowledge the support from KISTI Supercomputing Center (KSC-2007-S00-1006).

[1]C. S. Hwang, J. Appl. Phys. **92**, 432 (2002).
[2]O. G. Vendik, S. P. Zubko, and L. T. Ter-Martirosayn, Appl. Phys. Lett. **73**, 37 (1998).
[3]N. Nakaoka, K. Tada, S. Watanabe, H. Fujita, and K. Watanabe, Phys. Rev. Lett. **86**, 540 (2001).
[4]M. Stengel and N. A. Spaldin, Phys. Rev. B **75**, 205121 (2007).
[5]M. Stengel and N. A. Spaldin, Nature (London) **443**, 679 (2006).
[6]G. Kresse and J. Hafner, Phys. Rev. B **47**, 558 (1993); G. Kresse and J. Hafner, *ibid.* **49**, 14251 (1994).
[7]S. Baroni, A. Dal Corso, S. de Gironcoli, and P. Giannozzi, http://www.pwscf.org
[8]A. Balderschi, S. Baroni, and R. Resta, Phys. Rev. Lett. **61**, 734 (1988).
[9]F. Giustino and A. Pasquarello, Phys. Rev. B **71**, 144104 (2005).
[10]F. Giustino and A. Pasquarello, Phys. Rev. Lett. **95**, 187402 (2005).
[11]Y. Cho, C. Kim, H.-S. Ahn, E. Cho, T. Kim, and S. Han, J. Appl. Phys. **101**, 083710 (2007).
[12]B. Meyer and D. Vanderbilt, Phys. Rev. B **63**, 205426 (2001).
[13]P. E. Blöchl, Phys. Rev. B **50**, 17953 (1994).
[14]D. M. Ceperley and B. J. Alder, Phys. Rev. Lett. **45**, 566 (1980).
[15]L. Bengtsson, Phys. Rev. B **59**, 12301 (1999).
[16]Y. F. Dong, S. J. Wang, J. W. Chai, Y. P. Feng, and A. C. H. Huan, Appl. Phys. Lett. **86**, 132103 (2005).
[17]G.-M. Rignanese, F. Detraux, X. Gonze, and A. Pasquarello, Phys. Rev. B **64**, 134301 (2001).
[18]C. T. Black and J. J. Welser, IEEE Trans. Electron Devices **46**, 776 (1999).
[19]Ph. Ghosez, J.-P. Michenaud, and X. Gonze, Phys. Rev. B **58**, 6224 (1998).